Friction factor for aerosol fractal aggregates over the entire Knudsen range

James Corson,[1] George W. Mulholland,[1] and Michael R. Zachariah[1,2,*]

[1]*Department of Chemical and Biomolecular Engineering, University of Maryland, College Park, Maryland 20742, USA*

[2]*Department of Chemistry and Biochemistry, University of Maryland, College Park, Maryland 20742, USA*

We develop an approach for computing the hydrodynamic friction tensor and scalar friction coefficient for an aerosol fractal aggregate in the transition regime. Our approach involves solving the Bhatnagar-Gross-Krook equation for the velocity field around a sphere and using the velocity field to calculate the force on each primary sphere in the aggregate due to the presence of the other spheres. It is essentially an extension of Kirkwood-Riseman theory from the continuum flow regime to the entire Knudsen range (Knudsen number from 0.01 to 100 based on the primary sphere radius). Our results compare well to published direct simulation Monte Carlo results, and they converge to the correct continuum and free molecule limits. Our calculations for clusters with up to 100 spheres support the theory that aggregate slip correction factors collapse to a single curve when plotted as a function of an appropriate aggregate Knudsen number. This self-consistent-field approach calculates the friction coefficient very quickly, so the approach is well-suited for testing existing scaling laws in the field of aerosol science and technology, as we demonstrate for the adjusted sphere scaling method.

I. INTRODUCTION

Aerosol fractal aggregates formed from the coagulation of smaller, spherical primary particles are found in many natural and industrial settings. Understanding the forces on these aggregates is important in a number of science and engineering disciplines, including combustion, fire safety, atmospheric and environmental sciences, materials engineering [1], and nuclear reactor safety [2]. The translational drag force for a particle moving slowly relative to the surrounding fluid—given by $\boldsymbol{F} = -\zeta \boldsymbol{U}_0$, where $\boldsymbol{U}_0$ is the particle's relative velocity and ζ is the orientation-averaged scalar friction factor—is particularly important because it influences the transport properties of the particle, including its diffusion coefficient and electrical mobility.

In many practical applications, the primary sphere radius a is significantly less than the mean free path of the surrounding gas ($\lambda \approx 65$ nm at standard temperature and pressure and an order of magnitude higher near a flame), so that the primary sphere is in or near the free molecule flow regime. At the same time, the radius of gyration R_g for the agglomerate may be comparable to or larger than the mean free path, so that the aggregate is in the transition flow regime. As one example, for carbonaceous soot $a \approx 5$–30 nm and $R_g \approx 30$–1000 nm.

There are a number of theories and techniques for computing the translational friction factor of macromolecules and particle aggregates in the continuum regime, including Kirkwood-Riseman (KR) theory [3] and its extensions by Rotne and Prager [4], Yamakawa [5], and Chen *et al.* [6], as well as algorithms that use the Hubbard and Douglas analogy between the electrostatic capacitance and the friction factor [7–9]. Likewise, there are established methods for computing ζ in the free molecule regime that simulate the ballistic nature of interactions between gas molecules and aggregates [10–13].

In contrast, there are few approaches for the transition regime. Melas *et al.* [14] estimated the friction coefficient in the near-continuum regime by solving the Laplace equation with a slip boundary condition at the surface of the particle. In a followup paper, the authors determined that their collision rate method is valid for Knudsen numbers less than 2 [15].

Dahneke [16] developed the adjusted sphere method for the transition regime, which applies a slip correction factor to the continuum friction factor. The key to this development is the identification of an aggregate Knudsen number that reduces a problem involving two length scales (primary radius and aggregate radius of gyration) to a single dimensionless length. Dahneke's approach is similar to the approach used to calculate the drag on a sphere in the transition regime, but the adjusted sphere method uses an adjusted Knudsen number based on geometric descriptions of the particle in the continuum (hydrodynamic radius, R_H) and free molecular [projected area (PA)] regimes.

Through scaling analysis, Zhang *et al.* [17] developed an approach analogous to the adjusted sphere method and demonstrated that the approach yields friction factors comparable to direct simulation Monte Carlo (DSMC) results for the aggregates they studied (spheres, dimers, and dense and open 20-particle aggregates). However, it requires knowledge of the hydrodynamic radius and the projected area of the particle, which may take tens of minutes to a few hours to obtain computationally for a single particle. Obtaining R_H and PA experimentally is possible, but it requires painstaking transmission electron microscopy (TEM) measurements [18]. More rigorous computational techniques for calculating the transition regime friction factor—such as DSMC or molecular dynamics—are time-consuming: for instance, the reported DSMC calculation times in Ref. [17] were on the order of one CPU week for a given Knudsen number and a given aggregate. Thus, a self-consistent-field theory method for quickly estimating the scalar friction factor of an aggregate across the Knudsen range is highly desirable.

In this paper, we present an approach for computing the hydrodynamic friction tensor $\mathcal{H}$ and the scalar friction coefficient ζ for fractal aggregates across the entire Knudsen range. Our approach involves solving for the velocity field

*mrz@umd.edu

around a sphere in the transition regime and using the velocity field to compute the friction factor for the aggregate. In essence, this approach is an extension of KR theory [3] from the continuum regime to the transition regime. We will first present our solution of the Krook equation for the velocity field around a sphere, which follows the procedure developed by Lea and Loyalka [19] and Law and Loyalka [20]. We then describe our extension of KR theory to the transition regime. Finally, we compare our results to the DSMC results of Zhang *et al.* [17] and to the scaling theory in that paper.

II. VELOCITY FIELD

To determine the velocity around a sphere in the transition regime, we use the kinetic theory approach provided by the Boltzmann equation. For this study, we will use the Bhatnagar-Gross-Krook (BGK) model [21] instead of the full Boltzmann collision operator.

Consider a sphere with dimensional radius a^* in a gas moving at constant velocity $\boldsymbol{U}_\infty^*$. We will define the viscosity in terms of the gas mean free path λ as $\mu = 0.499\rho\bar{c}\lambda$, where $\bar{c}$ is the gas mean thermal speed, which is consistent with Ref. [17]. For this study, our nondimensional sphere radius is related to the Knudsen number $\text{Kn} = \lambda/a^*$ by $a = 0.501\sqrt{\pi}\,\text{Kn}^{-1}$ [22,23].

If the flow speed is very small compared to the thermal speed of the gas molecules ($U_\infty \ll 1$), then we can linearize the molecular velocity distribution $f(\boldsymbol{r},\boldsymbol{c})$,

$$f = \pi^{-3/2}\rho_\infty e^{-c^2}(1 + 2\boldsymbol{c}\cdot\boldsymbol{U}_\infty + h), \quad (1)$$

where ρ_∞ is the density far from the sphere, c is the molecular speed, and h is the perturbation to the distribution function due to the sphere. With this linearization and using the BGK model, we get the nondimensional Krook equation,

$$\boldsymbol{c}\cdot\nabla h(\boldsymbol{r},\boldsymbol{c}) = \varepsilon_1(\boldsymbol{r}) + \boldsymbol{c}\cdot\boldsymbol{\varepsilon}_2(\boldsymbol{r}) + \tfrac{2}{3}\left(c^2 - \tfrac{3}{2}\right)\varepsilon_3(\boldsymbol{r}) - h, \quad (2)$$

where ε_1, $\boldsymbol{\varepsilon}_2$, and ε_3 are perturbations to the density, velocity, and temperature fields around the sphere,

$$\rho(\boldsymbol{r}) = \rho_\infty[1 + \varepsilon_1(\boldsymbol{r})], \quad (3)$$

$$\boldsymbol{U}(\boldsymbol{r}) = \boldsymbol{U}_\infty + \tfrac{1}{2}\boldsymbol{\varepsilon}_2, \quad (4)$$

$$T(\boldsymbol{r}) = T_\infty[1 + \varepsilon_3(\boldsymbol{r})]. \quad (5)$$

We followed the same general solution procedure for the perturbations as Lea and Loyalka [19] and Law and Loyalka [20], with one exception related to the solution far from the sphere, as discussed below. Notably, we assumed diffuse reflection between the gas molecules and the sphere. This approach gives the r and θ components of the velocity perturbation $\boldsymbol{\varepsilon}_2$ as $U_0\sqrt{2}q_2(r)\cos\theta$ and $-U_0\sqrt{2}q_3(r)\sin\theta$, where r is the distance from the origin and θ is the angle between $\boldsymbol{r}$ and $\boldsymbol{U}_\infty$. The full velocity field in spherical coordinates is

$$\boldsymbol{U}(\boldsymbol{r}) = U_\infty\cos\theta\left[1 + \frac{1}{\sqrt{2}}q_2(r)\right]\mathbf{e_r}$$
$$- U_\infty\sin\theta\left[1 + \frac{1}{\sqrt{2}}q_3(r)\right]\mathbf{e_\theta}. \quad (6)$$
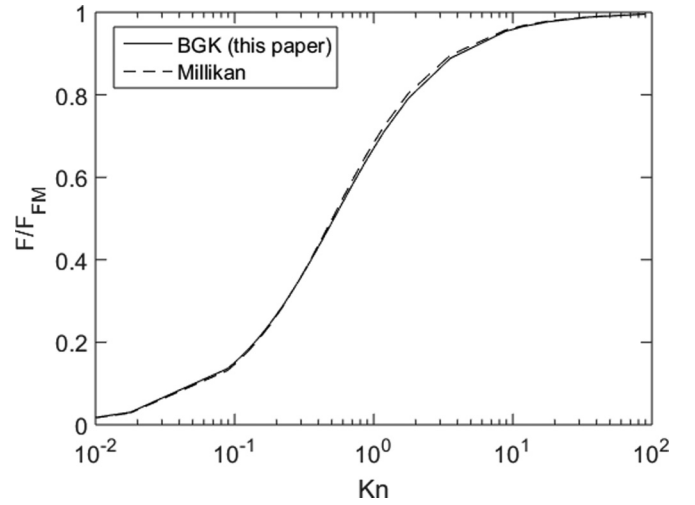
FIG. 1. Ratio of the calculated drag from the Krook equation to the free-molecule drag. Results are compared to a fit to Millikan's data [25].

Far from the sphere (i.e., for $r - a > 10$), we fit $q_2(r)$ and $q_3(r)$ to the asymptotic solution to the Krook equation given by Takata *et al.* [24],

$$\lim_{r\to\infty}q_2(r) = \sqrt{2}c_1\frac{a}{r} + \sqrt{2}c_2\left(\frac{a}{r}\right)^3, \quad (7)$$

$$\lim_{r\to\infty}q_2(r) = \frac{c_1}{\sqrt{2}}\frac{a}{r} - \frac{c_2}{\sqrt{2}}\left(\frac{a}{r}\right)^3. \quad (8)$$

Lea and Loyalka [19] and Law and Loyalka [20] used a slightly different form of the solution for large distances from the sphere, but otherwise our approach is consistent with the approach in Refs. [19,20].

We present our solution of the drag as the ratio between drag F for the specified Knudsen number and the free molecule drag F_{FM}. As shown in Fig. 1, our drag results compare favorably (i.e., within 2–3 %) with a fit to Millikan's oil drop data [25] reported by Cercignani *et al.* [23],

$$\frac{F}{F_{\text{FM}}} = \frac{A + B}{2\pi^{-1/2}a + A + B\exp(-2\pi^{-1/2}\text{Ca})}, \quad (9)$$

where $A = 1.234$, $B = 0.414$, and $C = 0.876$. Our results are also consistent with previous calculations [19,20,23,24], as shown in Table I. (See the Supplemental Material for more detailed results [26].)

III. KIRKWOOD-RISEMAN THEORY

Kirkwood and Riseman [3] demonstrated that the force on the ith element of an N-element polymer chain is given by

$$\boldsymbol{F}_i = -\zeta_0(\boldsymbol{U}_0 - \boldsymbol{u}_i) - \zeta_0\sum_{i\neq j}^n \mathbf{T}_{ij}\cdot\boldsymbol{F}_j, \quad (10)$$

where $\boldsymbol{U}_0$ is the unperturbed fluid velocity, $\boldsymbol{u}_i$ is the velocity of the ith chain element, ζ_0 is the friction factor given by Stokes' law, and $\mathbf{T}_{ij}$ is the hydrodynamic interaction tensor. The total

TABLE I. Comparison of our results for F/F_{FM} to Millikan's data and to results from previous computational studies.

a	Kn	Millikan [25]	Cercignani *et al.* [23]	Law and Loyalka [20]	This study
0.05	17.8	0.9784	0.9778	0.9771	0.9769
0.075	11.8	0.9677	0.9651	0.9658	0.9654
0.10	8.88	0.9571	0.9529	0.9546	0.9540
0.25	3.55	0.8959	0.8864	0.8912	0.8884
0.50	1.78	0.8036	0.7900	0.8007	0.7916
0.75	1.18	0.7236	0.7088	0.7271	0.7104
1.00	0.888	0.6549	0.6404	0.6513	0.6423
1.25	0.710	0.5961	0.5824	0.5967	0.5850
1.50	0.592	0.5456	0.5332	0.5507	0.5363
1.75	0.507	0.5021	0.4910	0.5115	0.4947
2.00	0.444	0.4645	0.4546	0.4779	0.4588
2.50	0.355	0.4029	0.3951	0.4233	0.4001
3.00	0.296	0.3551	0.3488	0.3521	0.3545
4.00	0.222	0.2863	0.2818	0.2870	0.2884
5.00	0.178	0.2396	0.2360	0.2431	0.2429
6.00	0.148	0.2058	0.2029	0.2120	0.2099
7.00	0.127	0.1804	0.1779	0.1822	0.1848
8.00	0.111	0.1606	0.1583	0.1642	0.1650
9.00	0.0987	0.1447	0.1426	0.1501	0.1492
10.00	0.0888	0.1317	0.1297	0.1388	0.1361

force on the chain is the vector sum of the forces on the chain elements, $\boldsymbol{F} = \sum_i^N \boldsymbol{F}_i$.

The original derivation used the Oseen tensor for $\mathbf{T}_{ij}$. Rotne and Prager [4] and Yamakawa [5] derived a modified hydrodynamic tensor $\mathbf{T}_{ij}$ that accounts for the curvature of the chain elements and hydrodynamic interactions between two elements,

$$\mathbf{T}_{ij} = \frac{1}{8\pi\mu r_{ij}}\left\{\left[\mathbf{I} + \frac{\boldsymbol{r}_{ij}\boldsymbol{r}_{ij}}{r_{ij}^2}\right] + \frac{2a^2}{3r_{ij}^2}\left[\mathbf{I} - \frac{3\boldsymbol{r}_{ij}\boldsymbol{r}_{ij}}{r_{ij}^2}\right]\right\}, \quad (11)$$

where $\boldsymbol{r}_{ij}$ is the vector from the ith element to the jth element, and r_{ij} is the distance between the elements. Chen, Deutch, and Meakin later applied this approach to find the translational drag force on a fractal aerosol particle [6,27,28].

Rotne and Prager [4] and Yamakawa [5] noted the similarities between their modified interaction tensor and the solution of Stokes flow around a stationary sphere. We can write the perturbation to the velocity caused by the sphere in the following form:

$$\boldsymbol{v}(\boldsymbol{r}_{ij}) = \mathbf{V}_{ij} \cdot \boldsymbol{U}_0, \quad (12)$$

where

$$\mathbf{V}_{ij}(\boldsymbol{r}_{ij}) = \frac{6\pi\mu a}{8\pi\mu r_{ij}}\left[\left(\mathbf{I} + \frac{\boldsymbol{r}_{ij}\boldsymbol{r}_{ij}}{r_{ij}^2}\right) + \frac{a^2}{3r_{ij}^2}\left(\mathbf{I} - \frac{3\boldsymbol{r}_{ij}\boldsymbol{r}_{ij}}{r_{ij}^2}\right)\right].$$
$$(13)$$

Written thus, the velocity perturbation is the dot product of the unperturbed velocity $\boldsymbol{U}_0$ and a tensor $\mathbf{V}_{ij}$ that describes the action of the sphere on the flow. $\mathbf{V}_{ij}$ is the product of the Stokes friction factor [the numerator of the leading coefficient in Eq. (13)] and a hydrodynamic tensor that is the same as the modified hydrodynamic interaction tensor in Eq. (11), with the exception of the factor of 2 in the r_{ij}^{-3} term in $\mathbf{T}_{ij}$. This suggests that we can replace the product $\zeta_0\mathbf{T}_{ij}$ in Eq. (10) with

the tensor $\mathbf{V}_{ij}$ with minimal error, since the term proportional to r_{ij}^{-3} decays quickly as we move further from the jth particle. The force on the ith particle is now

$$\boldsymbol{F}_i = -\zeta_0\boldsymbol{U}_0 - \sum_{i\neq j}^N \mathbf{V}_{ij} \cdot \boldsymbol{F}_j. \quad (14)$$

Here, we are assuming that each of the primary particles is translating at the same velocity relative to the background gas, which is appropriate for an aerosol particle. That relative velocity is now specified as $\boldsymbol{U}_0$.

To verify that the error in using the velocity perturbation tensor in place of the product of the modified Oseen tensor and the monomer friction coefficient is small, we calculated the drag on the open and dense 20-particle aggregates described below using both approaches. The error in the drag calculated using $\mathbf{V}_{ij}$ is less than 2% for the dense aggregate and less than 1% for the open aggregate. This error decreases as the number of primary spheres increases, as expected from the r_{ij}^{-3} dependence.

To extend KR theory from the continuum regime to the transition regime, we set ζ_0 equal to the friction coefficient for a sphere that we calculated using the Krook equation, and we write the hydrodynamic tensor $\mathbf{V}_{ij}$ in terms of the velocity perturbation $\boldsymbol{\varepsilon}_2$,

$$\mathbf{V}_{ij} = -\frac{q_2(r_{ij})}{\sqrt{2}}\frac{\boldsymbol{r}_{ij}\boldsymbol{r}_{ij}}{r_{ij}^2} - \frac{q_3(r_{ij})}{\sqrt{2}}\left(\mathbf{I} - \frac{\boldsymbol{r}_{ij}\boldsymbol{r}_{ij}}{r_{ij}^2}\right). \quad (15)$$

We obtain the orientation-averaged translational friction factor for the particle by following the approach outlined in Happel and Brenner [29]: we calculate $\boldsymbol{F}/\boldsymbol{U}_0$ for three mutually orthogonal particle orientations, compute the eigenvalues λ_m of the resulting friction tensor, and set the friction coefficient
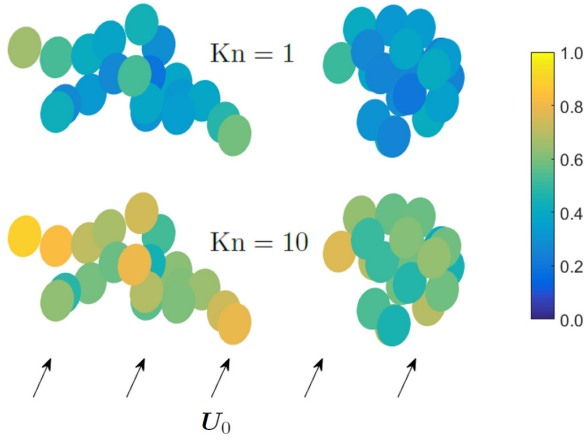
FIG. 2. Open (left) and dense (right) 20-particle aggregates used in this study. The calculated R_H and PA for these aggregates are very close to the values for the open and dense aggregates in Ref. [17]. The colors represent the calculated ratio of the drag on a primary sphere to the drag on an isolated sphere at the specified Knudsen number. A ratio of unity suggests that a sphere behaves as if it is isolated.

equal to the harmonic average of the eigenvalues,

$$\zeta = \left(\frac{1}{\lambda_1} + \frac{1}{\lambda_2} + \frac{1}{\lambda_3} \right)^{-1}. \tag{16}$$

Note that the friction tensor is symmetrical (allowing for some numerical uncertainty) in the transition regime, as it is in continuum flow.

Because our drag results from the Krook equation are nondimensionalized by the free-molecule drag force, we obtain the dimensional scalar friction factor by multiplying by the free-molecule friction factor for the primary sphere,

$$\zeta^* = \zeta \frac{\pi(8 + \pi)}{2.994} \frac{\mu}{\lambda} a^2. \tag{17}$$

IV. RESULTS

Numerous experimental studies have been performed to determine the friction coefficient—or a related quantity, the electrical mobility—for fractal aggregates in the transition regime, as summarized in a review paper by Sorensen [30]. However, most published data lack the detailed description of particle morphology (i.e., the hydrodynamic radius R_H and the PA) needed for a meaningful comparison with our theoretical calculations. Zhang *et al.* [17] compared DSMC results to their own data [31], while Thajudeen *et al.* [18] compared mobility data to the adjusted sphere method scaling law; both studies showed good agreement between theory and experimental data. Thus, we will compare our results to the scaling law and to published DSMC results [17] for well-characterized particles over a wide range of Knudsen numbers. Specifically, we have generated aggregates with similar characteristics to the open and dense aggregates in Ref. [17]. Our aggregates are shown schematically in Fig. 2. We generated the particles with a cluster growth algorithm [13] where we specify the fractal prefactor and exponent and the number of primary spheres. We verified that our particles have similar hydrodynamic radii and projected areas to the
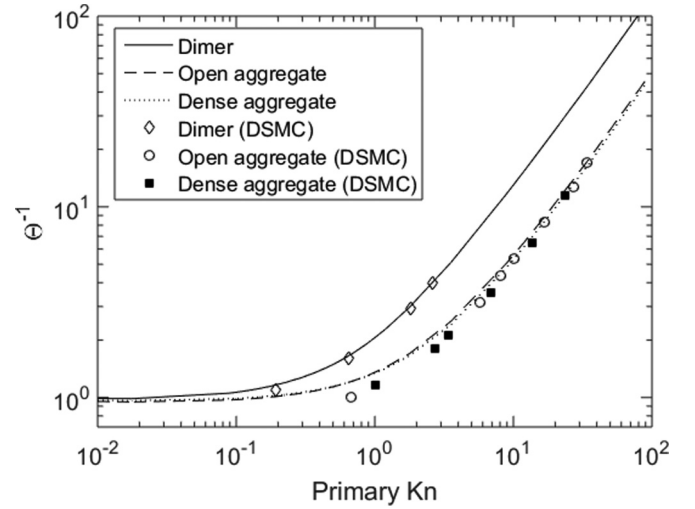
FIG. 3. Comparison of our results for the slip correction factor to the DSMC results from Zhang *et al.* [17] for a dimer, an open 20-particle aggregate, and a dense 20-particle aggregate. The slip correction factor is the ratio of the continuum friction factor $6\pi\mu R_H$ to the calculated friction factor.

particles described in Ref. [17] using the Zeno algorithm [32] for R_H and our own algorithm for the projected area. (The Zeno algorithm uses a random-walk approach to calculate the electrostatic capacity of an aggregate; Hubbard and Douglas [7] have demonstrated that the hydrodynamic radius is within 1% of the electrostatic capacity for shapes with analytical solutions for both quantities.) We also compared our results for a dimer to the DSMC results.

Figure 2 illustrates the effects of the Knudsen number on the flow field and drag on each primary sphere. The color of each sphere in the figure is the ratio between the calculated drag F_i on each sphere and the drag $\zeta_0 U_0$ on an isolated sphere at the specified Knudsen number; alternatively, the color represents the fluid velocity at the center of each sphere. The open aggregate at a primary Knudsen number of 10 has relatively little effect on the flow field. Monomers near the periphery of the aggregate behave almost like isolated spheres, while monomers near the interior of the particle experience a lower fluid velocity largely due to direct shielding by the other spheres. This behavior is characteristic of free-molecule flow.

For the same particle at a primary Knudsen number of 1, the velocity at each monomer is much lower than in the Kn = 10 case. Clearly, all of the monomers are affected to a larger degree by the presence of the neighboring spheres. The same is true for the dense aggregates with a fractal dimension of 2.5: each monomer has more neighbors, and thus each monomer behaves less like an isolated sphere than in the case of an open aggregate with a fractal dimension of 1.78.

Our results for the drag on the dimer and open and dense aggregates are shown in Fig. 3. Here, we have plotted the aggregate slip correction factor, $\Theta^{-1} = 6\pi\mu R_H/\zeta^*$, versus the primary Knudsen number. Both our results and the DSMC results assume diffuse reflection and full thermal accommodation between the gas molecules and the particle. In general, our KR theory results compare well with the DSMC results. Our calculated slip correction factors are higher
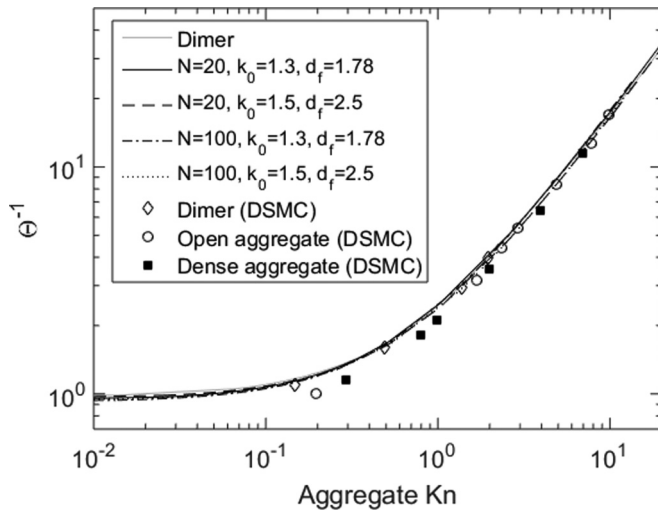
FIG. 4. Calculated slip correction factors for a range of aggregate morphologies, plotted vs the aggregate Knudsen number. DSMC results from Zhang *et al.* [17] are included for comparison.

than the DSMC slip factors at decreasing Knudsen numbers, though Zhang *et al.* [17] note that their DSMC results tend to underpredict the slip correction factor due to the finite size of the computational domain. The DSMC results are particularly influenced by domain size at lower Knudsen numbers, which explains the larger deviation between our results and the DSMC results in the near-continuum regime. Note that we discarded one of the near-continuum dense aggregate DSMC points from Ref. [17] because it fell significantly below the continuum limit $\Theta^{-1} = 1$.

We used our Kirkwood-Riseman approach to test the observations put forth in Refs. [17,18,33] that plots of the slip correction factor versus the aggregate Knudsen number, defined by Zhang *et al.* [17] as

$$\mathrm{Kn} = \pi \lambda R_H / PA, \tag{18}$$

collapse to a single curve. Figure 4 shows our results for aggregates with a range of fractal dimensions and the number of primary spheres. We also include the DSMC results from Zhang *et al.* [17] for comparison. Our results and the DSMC results all follow the same general curve, with relatively little deviation among the various calculations. This provides further

support to the theory of a universal slip correction factor versus aggregate Knudsen number scaling law.

V. DISCUSSION

We have introduced an approach for computing the translational friction coefficient for a fractal aerosol particle across the entire Knudsen range, given the particle's coordinates and primary sphere radius. Coordinates can be generated using a cluster growth algorithm, as we have done for this study, or they can be obtained from TEM images using methods described in the literature (see, e.g., Ref. [18]).

The solution method is also very fast: it takes approximately 10 s on a single processor to obtain the friction coefficient for approximately 50 Knudsen numbers for a 20-particle aggregate. Furthermore, our Kirkwood-Riseman results converge to the correct continuum and free-molecule limits obtained using the Hubbard-Douglas approximation for the continuum and a ballistic approach for the free-molecule aggregate friction factor.

Over the parameter range examined, our results support the validity of the adjusted sphere method developed by Dahneke [16] and Zhang *et al.* [17] and promoted by more recent studies [14,15,18,33]. Because the Kirkwood-Riseman approach can provide results quickly across the Knudsen range, this approach may be preferable to DSMC for evaluating scaling laws (such as those developed by Rogak *et al.* [34], Lall and Friedlander [35], and Eggersdorfer *et al.* [36]) that relate the friction coefficient to the number of primary spheres in the aggregate.

While we have focused on the friction coefficient in this paper, our method also determines the friction tensor, which is important when considering particle alignment in an external force field [37].

Finally, we emphasize that our results assume diffuse reflection between the gas molecules and the particle. This is consistent with past computational studies for fractal aerosol particles (see, e.g., Refs. [13,17]) and with experimental results, which suggest that most collisions are diffuse [38]. With that said, the Kirkwood-Riseman approach could be applied for alternative reflection models, provided one solves the Krook equation for the velocity using the appropriate boundary condition at the surface of the sphere.

[1] S. Friedlander, *Smoke, Dust, and Haze: Fundamentals of Aerosol Dynamics*, 2nd ed., Topics in Chemical Engineering (Oxford University Press, New York, 2000).

[2] S. Loyalka, Prog. Nucl. Energy **12**, 1 (1983).

[3] J. G. Kirkwood and J. Riseman, J. Chem. Phys. **16**, 565 (1948).

[4] J. Rotne and S. Prager, J. Chem. Phys. **50**, 4831 (1969).

[5] H. Yamakawa, J. Chem. Phys. **53**, 436 (1970).

[6] Z.-Y. Chen, J. Deutch, and P. Meakin, J. Chem. Phys. **80**, 2982 (1984).

[7] J. B. Hubbard and J. F. Douglas, Phys. Rev. E **47**, R2983 (1993).

[8] H.-X. Zhou, A. Szabo, J. F. Douglas, and J. B. Hubbard, J. Chem. Phys. **100**, 3821 (1994).

[9] J. F. Douglas, H.-X. Zhou, and J. B. Hubbard, Phys. Rev. E **49**, 5319 (1994).

[10] P. Chan and B. Dahneke, J. Appl. Phys. **52**, 3106 (1981).

[11] P. Meakin, B. Donn, and G. W. Mulholland, Langmuir **5**, 510 (1989).

[12] A. A. Shvartsburg and M. F. Jarrold, Chem. Phys. Lett. **261**, 86 (1996).

[13] D. W. Mackowski, J. Aerosol Sci. **37**, 242 (2006).

[14] A. D. Melas, L. Isella, A. G. Konstandopoulos, and Y. Drossinos, Aerosol Sci. Technol. **48**, 1320 (2014).

[15] A. D. Melas, L. Isella, A. G. Konstandopoulos, and Y. Drossinos, J. Aerosol Sci. **82**, 40 (2015).

[16] B. E. Dahneke, J. Aerosol Sci. **4**, 163 (1973).

[17] C. Zhang, T. Thajudeen, C. Larriba, T. E. Schwartzentruber, and C. J. Hogan, Jr., Aerosol Sci. Technol. **46**, 1065 (2012).

[18] T. Thajudeen, S. Jeon, and C. J. Hogan, J. Aerosol Sci. **80**, 45 (2015).

[19] K. Lea and S. Loyalka, Phys. Fluids **25**, 1550 (1982).

[20] W. Law and S. Loyalka, Phys. Fluids **29**, 3886 (1986).

[21] P. L. Bhatnagar, E. P. Gross, and M. Krook, Phys. Rev. **94**, 511 (1954).

[22] C. Cercignani and C. Pagani, Phys. Fluids **11**, 1395 (1968).

[23] C. Cercignani, C. Pagani, and P. Bassanini, Phys. Fluids **11**, 1399 (1968).

[24] S. Takata, Y. Sone, and K. Aoki, Phys. Fluids A **5**, 716 (1993).

[25] R. A. Millikan, Phys. Rev. **22**, 1 (1923).

[26] See Supplemental Material at http://link.aps.org/supplemental/10.1103/PhysRevE.95.013103 for our calculated velocity and drag results.

[27] P. Meakin, Z.-Y. Chen, and J. Deutch, J. Chem. Phys. **82**, 3786 (1985).

[28] P. Meakin and J. M. Deutch, J. Chem. Phys. **86**, 4648 (1987).

[29] J. Happel and H. Brenner, *Low Reynolds Number Hydrodynamics: With Special Applications to Particulate Media*, Prentice-Hall International Series in the Physical and Chemical Engineering Sciences (Prentice-Hall, Englewood Cliffs, NJ, 1965).

[30] C. M. Sorensen, Aerosol Sci. Technol. **45**, 765 (2011).

[31] K. Cho, C. J. Hogan, Jr., and P. Biswas, J. Nanopart. Res. **9**, 1003 (2007).

[32] M. L. Mansfield, J. F. Douglas, and E. J. Garboczi, Phys. Rev. E **64**, 061401 (2001).

[33] R. Gopalakrishnan, P. H. McMurry, and C. J. Hogan, J. Aerosol Sci. **82**, 24 (2015).

[34] S. N. Rogak, R. C. Flagan, and H. V. Nguyen, Aerosol Sci. Technol. **18**, 25 (1993).

[35] A. A. Lall and S. K. Friedlander, J. Aerosol Sci. **37**, 260 (2006).

[36] M. Eggersdorfer, A. Gröhn, C. Sorensen, P. McMurry, and S. Pratsinis, J. Colloid Interface Sci. **387**, 12 (2012).

[37] M. Li, G. W. Mulholland, and M. R. Zachariah, Aerosol Sci. Technol. **46**, 1035 (2012).

[38] P. S. Epstein, Phys. Rev. **23**, 710 (1924).